Zhou, X., **Jomaa, S.**, **Yang, X.**, **Merz, R.**, Wang, Y., **Rode, M.** (2022):
Exploring the relations between sequential droughts and stream nitrogen dynamics in central Germany through catchment-scale mechanistic modelling
J. Hydrol. **614, Part B** , art. 128615

https://doi.org/10.1016/j.jhydrol.2022.128615

Exploring the relations between sequential droughts and stream nitrogen dynamics in central Germany through catchment-scale mechanistic modelling

Xiangqian Zhou[a,*], Seifeddine Jomaa[a], Xiaoqiang Yang[a,b], Ralf Merz[c], Yanping Wang[d], Michael Rode[a,e]

[a]Department of Aquatic Ecosystem Analysis and Management, Helmholtz Centre for Environmental Research-UFZ, Magdeburg, Germany

[b]Department of Ecohydrology and Biogeochemistry, Leibniz Institute of Freshwater Ecology and Inland Fisheries (IGB), Berlin, Germany

[c]Department Catchment Hydrology, Helmholtz Centre for Environmental Research-UFZ, Halle (Saale), Germany

[d]School of Geographical Science, Nantong University, Nantong, China

[e]Institute of Environmental Science and Geography, University of Potsdam, Potsdam-Golm, Germany

[*]Corresponding author: Xiangqian Zhou (xiangqian.zhou@ufz.de)

Abstract

Like many other regions in central Europe, Germany experienced sequential summer droughts from 2015-2018. As one of the environmental consequences, river nitrate concentrations have exhibited significant changes in many catchments. However, catchment nitrate responses to the changing weather conditions have not yet been mechanistically explored. Thus, a fully distributed, process-based catchment Nitrate model (mHM-Nitrate) was used to reveal the causal relations in the Bode catchment, of which river nitrate concentrations have experienced contrasting trends from upstream to downstream reaches. The model was evaluated using data from six gauging stations, reflecting different levels of runoff components and their associated nitrate-mixing from upstream to downstream. Results indicated that the mHM-Nitrate model reproduced dynamics of daily discharge and nitrate concentration well, with Nash-Sutcliffe Efficiency ≥ 0.73 for discharge and Kling-Gupta Efficiency ≥ 0.50 for nitrate concentration at most stations. Particularly, the spatially contrasting trends of nitrate concentration were successfully captured by the model. The decrease of nitrate concentration in the lowland area in drought years (2015-2018) was presumably due to (1) limited terrestrial export loading (ca. 40% lower than that of normal years 2004-2014), and (2) increased in-stream retention efficiency (20% higher in summer within the whole river network). From a mechanistic modelling perspective, this study provided insights into spatially heterogeneous flow and nitrate dynamics and effects of sequential droughts, which shed light on water-quality responses to future climate change, as droughts are projected to be more frequent.

Keywords

Drought; Nitrate mixing; Catchment hydrology; Water quality model

Highlights:

- The model reproduces nitrate dynamics and trends under changing weather conditions.
- Nitrate dynamics show spatiotemporally varying responses to the sequential droughts.
- Soil export decreases while in-stream retention efficiency increases in droughts.

1. Introduction

Central Europe recently experienced sequential droughts in 2013, 2015, 2018 and 2019 (Hanel et al., 2018; Hari et al., 2020), and droughts are projected to become more frequent and severe in the future (Hari et al., 2020; Spinoni et al., 2018). In Germany, mean annual temperature increased by 1.5°C from 1881-2018, with ca. 0.3°C of that increase occurring from 2014-2018 (UBA, 2019). Using an ensemble of climate-change scenarios, Huang et al. (2015) reported that most rivers in Germany will experience more frequent droughts.

Excess nitrogen (N) input to surface water due to intensive anthropogenic activities (e.g., fertiliser application from arable land, wastewater from urban and industrial areas) has caused widespread environmental problems in recent decades. Nitrate turnover processes at the catchment scale are expected to change due to climate change (Hesse and Krysanova, 2016; Mosley, 2015; Whitehead et al., 2009), especially due to an increase in drought events (Ballard et al., 2019; Zwolsman and van Bokhoven, 2007).

The influence of drought on N dynamics has received increasing attention in recent decades (e.g., Baldwin et al., 2005; Lutz et al., 2016; Mosley, 2015; van Vliet and Zwolsman, 2008; Whitehead et al., 2009; Yevenes et al., 2018; Zwolsman and van Bokhoven, 2007). Previous studies have reported decreasing nitrate concentration in response to drought, for example, in the Meuse River in western Europe (van Vliet and Zwolsman, 2008), which was attributed to less diffuse input during drought periods. During a drought in Chile from 2010-2015, Yevenes et al. (2018) found that nitrate concentration did not change in the upstream part of a study catchment but decreased downstream due to differences in discharge regime and nitrate sources from upstream to downstream. In line with these findings, numerous studies have reported that droughts can have spatiotemporally varying impacts on nitrate transport and transformation processes due to the heterogeneous changes in hydrological processes within catchments (e.g., Leitner et al., 2020; Lintern et al., 2018; Lutz et al., 2016). These studies are generally based on data-driven and statistical analyses, but conclusions drawn from them are site-specific and often do not provide a full understanding of the factors that influence the effects of drought on nitrate dynamics and their spatial heterogeneity. Thus, it is crucial to identify the mechanisms that underlie water-quality trends under drought conditions to ensure future water quality and develop effective management strategies. Furthermore, the scientific understanding gained from analysing deterministic trends can help to predict future trends. However, how sequential droughts influence stream nitrate responses has not yet been mechanistically explored. Catchment-scale hydrological water-quality models are an alternative solution to identify the relations between changing weather conditions and changes in nitrate dynamics. These models can reproduce catchment nitrate dynamics and stream water concentrations well based on hydrological understanding, which can be transferred across catchments or climate conditions (Jiang et al., 2014; Wellen et al., 2015). Process-based water-quality models are rarely used to investigate spatiotemporal effects of historical droughts on N concentrations at the catchment scale. One of the challenges is to adequately represent the catchment spatial heterogeneity and the complexity of nitrate dynamic processes, which can become more important during droughts (Rode et al., 2010; Wellen et al., 2015). The fully distributed hydrological model mHM (Samaniego et al., 2010) introduces flexible multiscale catchment discretization and parameterization techniques. The mHM-Nitrate model was recently developed based on the hydrological mHM platform, including advanced descriptions of terrestrial and in-stream nitrate processes and consideration of agricultural management (Yang et al., 2018). The model has shown a robust ability to provide reliable, detailed information about terrestrial and in-stream nitrate dynamics (Yang et al., 2019a; Yang et al., 2019b; Yang et al., 2018). Thus, the model acts as a promising tool for mechanistic investigation of the impacts of drought on stream nitrate dynamics. In this study, we applied mHM-Nitrate to the Bode catchment (3200 km^2, central

Germany; part of the German TERENO observatories). The catchment has large hydroclimatic, geophysical and landscape gradients and has experienced sequential droughts in recent years (2015-2018). The objectives of the study were to (i) simulate spatiotemporal nitrate dynamics in a mesoscale catchment with widely differing meteorological and land-use characteristics using the mHM-Nitrate model, (ii) evaluate mHM-Nitrate's ability to represent recent drought-induced trends in nitrate concentration and (iii) analyse mechanisms that influence spatiotemporally varying river nitrate concentrations under sequential droughts.

2. Materials and Methods

2.1 Study area

The Bode catchment is an intensively monitored and investigated mesoscale catchment in central Germany (Wollschläger et al., 2016) (Figure 1). The catchment includes the Harz Mountains in the southwest and lowland plains in the northeast. Elevation of the catchment ranges from 1142 m.a.s.l. at the Brocken (the highest peak of the Harz Mountains) to 70 m.a.s.l. in the lowland area. Along the elevation gradient, the catchment has large gradients of meteorological, land use, soil type and geological characteristics. Annual mean precipitation varies from more than 1500 mm at the Brocken to ca. 500 mm in the lowland (Wollschläger et al., 2016). Mean annual potential evapotranspiration is around 710 mm in the mountain area while it is about 810 mm in the lowland area. Mean annual temperature ranges from 5°C on the Brocken to 9.5°C in the lowland, with a minimum of -0.6°C (1.2°C) in January and a maximum of 16.8°C (19.1°C) in July in the mountain and lowland area, respectively. The Bode catchment experienced sequential summer droughts from 2015-2018 according to the 3-month standardized precipitation evapotranspiration index (Vicente-Serrano et al., 2010) (Figure S1). Land use in the mountain area is dominated by forest, with 10% pasture, 8% agriculture and 7% urban areas and lakes. The soil type in the Harz Mountains is dominated by Cambisols. Land use in the lowland area is dominated by agriculture (81%), whose main crops are winter wheat, winter barley, rapeseed and sugar beet; forest and pasture cover 7% and 3%, respectively; and urban areas and small lakes cover the remaining 9% (Figure 1b). Chernozems are the main soil type in the lowland area.

To classify typical landscape nitrate-leaching behaviour of agricultural soils, five dominant soil classes were identified (Figure 1c) according to the United States Department of Agriculture classification by combining soil properties and land-use types: sandy, silt loam, silty clay loam and loam. In the mountain forest area N input is restricted to atmospheric deposition and nitrate export amounts in this area are very low, we restricted the soil-land-use class N-balance analysis to agricultural soils. Then, these classes on the soil texture map were intersected with the land-use map, and the cells in which the area of the dominant soil-land-use class exceeded 80% of the cell's area were selected. Consequently, the lowland area was classified into Classes I-III, which represented the dominant loess area (silt loam soils), riverine area (loam soils) and highly sandy area (sandy soils), respectively. Two representative classes in the mountain area were selected: Class IV, which represented the mountain pasture area (silty clay loam soils), and Class V, which represented the mountain arable area (sandy soils).

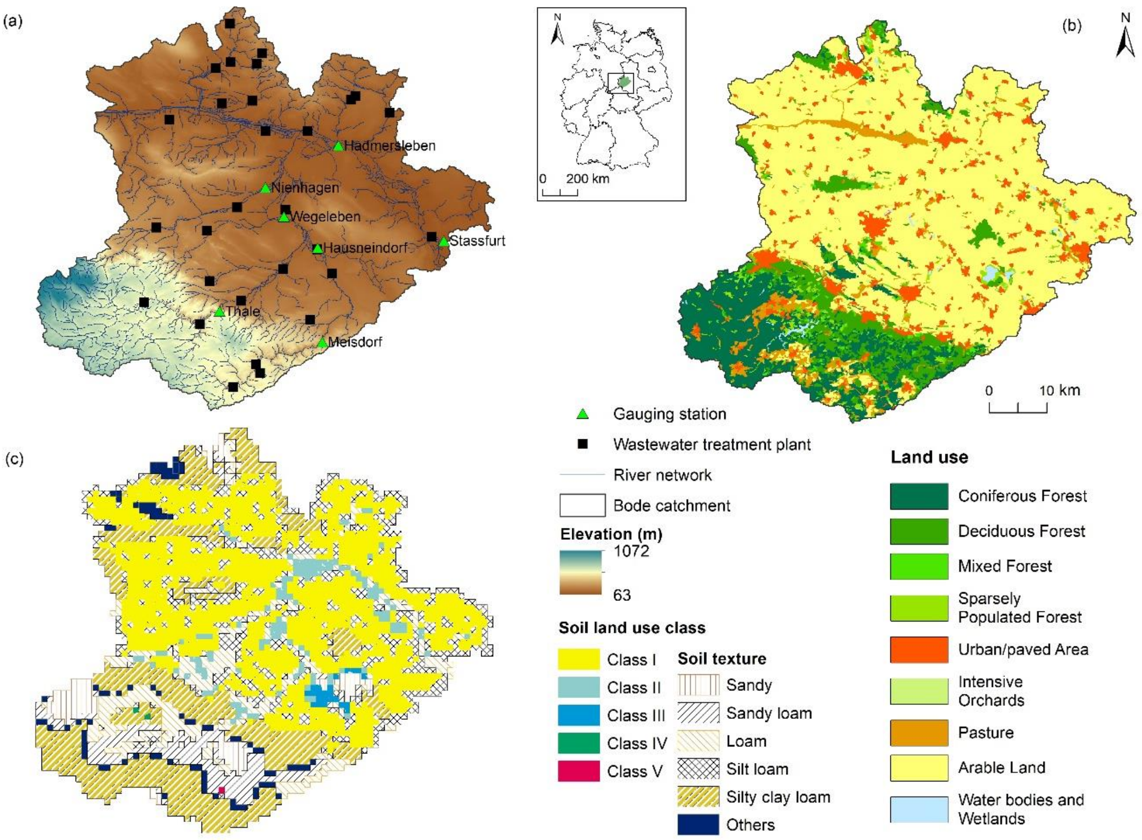

Figure 1. The Bode catchment: (a) geographical location of the gauging stations and wastewater treatment plants, (b) land use types and (c) five dominant soil-land-use classes.

2.2 Data availability

Meteorological data were derived from the German Weather Service (DWD), including daily precipitation and daily mean temperature from 2000-2018. To create the meteorological forcing inputs for the model, the DWD observations were spatially interpolated into 1 km × 1 km grid data, using the kriging method drifted by terrain elevation. This method considers the orographic effect on precipitation and temperature by using the elevation as an external variable for the interpolation (Hundecha and Bárdossy, 2004). Daily potential evapotranspiration data were calculated using the Hargreaves and Sammi (1985) method at the same spatial resolution.

A terrain elevation model was obtained from the Shuttle Radar Topography Mission (SRTM) sensor (Jarvis, 2008). The digitized geological map and soil map, both at a scale of

1:1,000,000, were obtained from the Federal Institute for Geosciences and Natural Resources (BGR) (https://produktcenter.bgr.de, last accessed 1 June 2020). Land-cover data were derived from CORINE Land Cover 10 ha (https://gdz.bkg.bund.de/index.php/default/open-data.html, last accessed 1 June 2020). These datasets were resampled to a spatial resolution of 100 m × 100 m for model simulations.

Data on mineral fertiliser and manure application rates and times, as well as crop rotations on arable land, were obtained from the model configuration of Yang et al. (2018) and agricultural authorities (https://llg.sachsen-anhalt.de/llg/, last accessed 10 April 2020). The total amount of fertiliser (mineral fertiliser and manure) applied depended on crop type and was assumed to be applied evenly throughout the fertilisation period. The resolution of the crop-rotation map was set to that of the land-use map for technical simplification due to the lack of detailed information. Point-source data were collected from Urban Wastewater Treatment Directive (UWWTD) sites for Germany (https://uwwtd.eu/Germany/uwwtps/treatment, last accessed 10 April 2020). Overall, 29 wastewater treatment plants (WWTPs) were considered (Figure 1a). The original point-source data were available only as annual total N load. Based on detailed authority data from large wastewater treatment plants' outflow, values of NH4 were always below 1.0 mg N L^{-1} (mostly below 0.1 mg N L^{-1}) and total NO3 ranged between 2 and 12 mg N L^{-1}. Higher NH4-N values correspond to higher NO3-N values. Furthermore, NH4 is quickly processed to NO3 within the streams (Rahimi et al., 2020). Thus, in our catchment nitrate is the main form of N from WWTPs, and the daily inputs were obtained by dividing annual total N load by the number of days in that year. The percentage of point-source N load, which was calculated by dividing the annual total N load of the 29 WWTPs by the observed annual nitrate-N load at the catchment outlet station, equalled only 12% of the total N load in the Bode catchment during the study period.

Daily discharge at six gauging stations (Meisdorf, Hausneindorf, Wegeleben, Nienhagen, Hadmersleben and Stassfurt) was provided by the State Agency for Flood Protection and Water Management of Saxony-Anhalt (LHW) (http://gldweb.dhi-wasy.com/gld-portal/, last accessed 10 April 2020). Nitrate concentration was measured twice weekly to twice monthly from 2000-2009 by LHW (http://gldweb.dhi-wasy.com/gld-portal/, last accessed 10 April 2020) and daily from 2010-2018 by the Helmholtz Centre for Environmental Research – UFZ. Nitrate concentration observations were missing for 2015 and 2017-2018 at the Wegeleben station, and discharge observations were missing for 2017-2018 at the Nienhagen station (Figure 1a).

2.3 mHM-Nitrate model description

The mHM-Nitrate model is a grid-based catchment nitrate model that balances process complexity and model representation (Yang et al., 2018). Nitrate-process descriptions come mainly from the HYPE model (Lindström et al., 2010), with additional considerations of nitrate retention in deep groundwater, spatially distributed crop rotations and time-varying point-source inputs. The model includes the following hydrological processes: canopy interception, snow accumulation and melt, evapotranspiration, infiltration, soil moisture dynamics, runoff generation, percolation and flood routing along the river network. Nitrate processes are fully integrated into the hydrological cycling. Major N inputs include wet atmospheric deposition via precipitation, fertiliser and manure application and plant/crop residues. In each soil layer, four N pools are defined (i.e., active solid organic N, inactive solid organic N, dissolved organic N and dissolved inorganic N), along with soil N processes of denitrification, plant/crop uptake and transformations among the four N pools. In-stream N transformations include denitrification, primary production and mineralization. Governing equations of N transformations in the soil and the stream can be found in Supplementary material (Text S1). More detailed descriptions of the mHM-Nitrate model can be found in Yang et al. (2018), and source code can be found in Yang and Rode (2020).

2.4 Model calibration and performance measurements

The mHM-Nitrate model was set at a daily time step from 2000-2018 (2000-2003 was considered a warm-up period). We used daily discharge and nitrate concentration data from 2010-2014 as calibration data. The nitrate concentration data used to validate model predictions included twice weekly to twice monthly grab sampling data for 2004-2009 and daily data for 2015-2018. To minimize the influence of the Rappbode reservoir in the upper Bode River, observed discharge and nitrate concentration at the Thale station were used as the input flow and nitrate concentration when setting up the model.

Before calibrating the model, sensitivity analysis was performed to identify the most influential parameters using the Morris method (Morris, 1991). Parameter samples were generated using radial-based Latin-Hypercube sampling, and 200 trajectories were set to ensure convergence of the sensitivity analysis. Sensitivity indices (absolute mean (μ) and standard deviation (σ) of each parameter's elementary effect) were calculated using the SAFE tool (Sensitivity Analysis For Everybody, (Pianosi et al., 2015)). The sensitivity ranking was obtained by plotting μ vs. σ for all parameters; the more to the right and top of the plot a point is located, the more the parameter is influential and interrelated with other parameters, respectively. The Dynamically Dimensioned Search (DDS) method (Tolson and Shoemaker, 2007) was used to calibrate the most influential parameters, with 50,000 iterations as the terminal criterion. The detailed procedure of parameter sensitivity analysis and calibration can be found in Yang et al. (2018).

The multi-objective function for calibration consisted of multi-criteria, multi-site and multi-variable functions. We selected the Nash-Sutcliffe Efficiency (NSE) and the logarithm-transformed NSE (lnNSE) as objective criteria, in which the latter gives more weight to low values. The combined NSE and lnNSE as objective criteria increase the potential to find a robust parameter set for both high flow and low flow. In addition, six internal gauging stations were considered to calibrate discharge and nitrate concentrations simultaneously, with a weight-aggregated multi-variable function, as follows:

$$OF_{mutil-v} = min\{w_q OF_{mutil-s}^{q} + w_n OF_{mutil-s}^{n}\} \quad (1)$$

where $OF_{mutil-s}^{q}$ and $OF_{mutil-s}^{n}$ denote multi-site objective functions, which are the unweighted sum of NSE and lnNSE across all six gauging stations for discharge and nitrate concentration, respectively; and w_q= 0.9 and w_n= 0.1 denote weights for discharge and nitrate concentration objectives, respectively. Three goodness-of-fit metrics were used to evaluate model performance: NSE, Kling-Gupta Efficiency (KGE) and Percentage BIAS (PBIAS) (e.g., Gupta et al., 2009; Moriasi et al., 2015).

2.5 Trend analysis

To further validate the mHM-Nitrate model capability to capture the trend caused by the drought, we compared the trend components between observed and simulated discharge and nitrate concentration. Observed discharge and nitrate concentration time series at the six gauging stations were first aggregated into a monthly time step to minimize effects of different observation frequencies. Missing values in the observed nitrate time series were interpolated using the Kalman smoothing method in the R package *imputeTS* (version 4.0.2) (R Core Team., 2020). Each time series, Y_t (i.e., monthly nitrate or discharge) was then broken down into trend, seasonality and random components using the following equation:

$$Y_t = T_t + S_t + e_t \quad (2)$$

where T_t is the trend component, S_t is the seasonal component and e_t is a random component, which represents residuals.

The trend component was determined from a moving average with a symmetric window (window size =19) using the STL function (Cleveland, 1990) in the R package *stats* (version 4.0.2), which has been successfully used to analyse seasonal and long-term nitrate trends (Stow et al., 2014, 2015). The STL algorithm consists of two iterative loops, the inner and outer loops. In the inner loop, the time series is first de-trended: T_t is extracted and smoothed with a local fitting with weights applied to the points that are fitted. Then the seasonal component is extracted using a low-pass filter. In the outer loop, the residuals e_t is used to create robustness weights for the next round of the inner loop. These robustness weights reflect how extreme the residuals are. As the outliers in the time series Y_t result in large residuals, the outliers will have small or zero weight (Cleveland, 1990). The trends of monthly discharge and nitrate concentration were then normalized using min-max normalization. The significance of normalized trend components of monthly discharge and nitrate concentration was analysed by using Mann-Kendall trend test, which was performed using the mk.test function in the R package *trend* (version 1.1.4).

3. Results

3.1 Sensitivity results

In this study, the mHM-Nitrate model included 72 parameters (61 for hydrological processes and 11 for nitrate processes). Simultaneous parameter sensitivity analysis showed that hydrological predictions were the most sensitive (Figure 2). Predictions of runoff were most sensitive to pet1 (the terrain-aspect correction of potential evapotranspiration), sm10 (the transfer function used to calculate soil saturated hydraulic conductivity) and sm17 (used to calculate the fraction of water that infiltrates through soil layers).

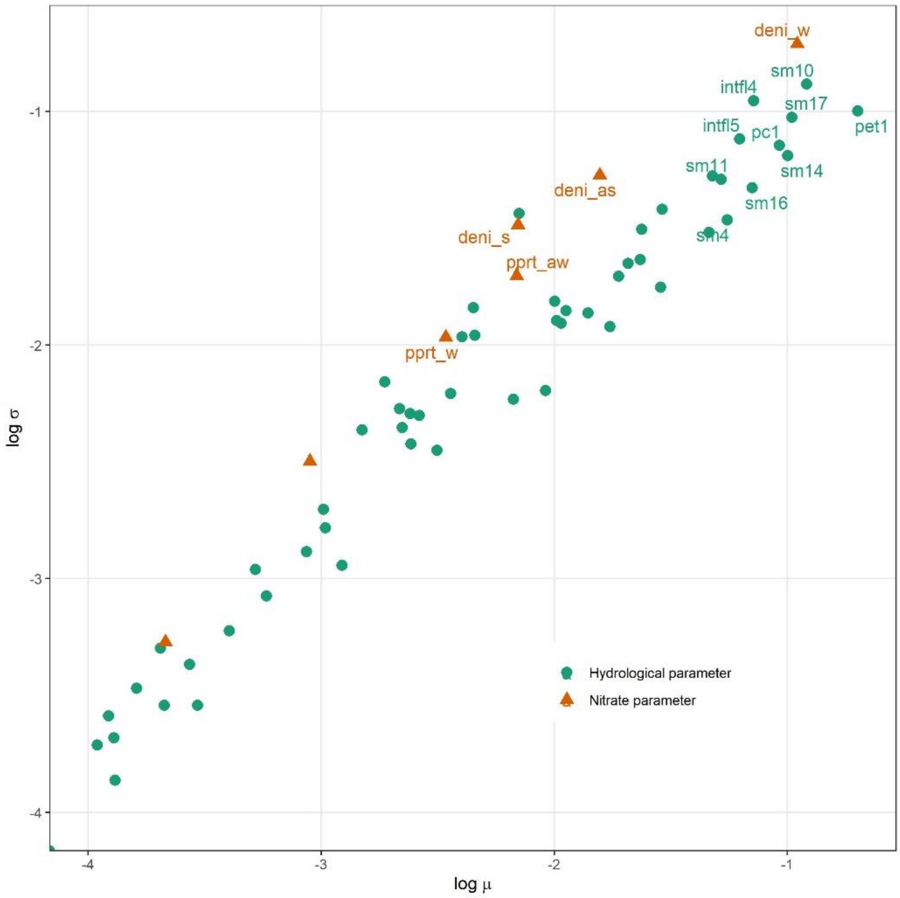

Figure 2. Simultaneous parameter sensitivity ranking of the 60 most influential parameters of the mHM-Nitrate model. The 16 labelled parameters (the top 10 hydrological and 6 nitrate parameters, respectively) are related to soil moisture (sm), evapotranspiration (pet), interflow generation (intfl), soil denitrification rates in the arable area (deni_as) and non-arable area (deni_s), mineralization rate in the arable area (miner_a), in-stream denitrification rates (deni_w) and in-stream primary production rate in the arable area (pprt_aw) and non-arable area (pprt_w). See Table 1 for additional definitions. The more a point is near the right and top of the plot, the more the parameter is influential and interrelated with other parameters, respectively, μ and σ is the absolute mean and standard deviation of each parameter's elementary effect. Note the log-log scales.

For nitrate submodel, the most sensitive parameters were the in-stream denitrification rate (deni_w) (for the entire Bode stream network) and two land-use parameters (deni_as and deni_s) (soil denitrification rate in the agricultural and non-agricultural areas, respectively) (Table 1). In line with the results of Yang et al. (2018) and Cuntz et al. (2015), the two most influential parameters for hydrological predictions were pet1 and sm10. Generally, the larger the associated flux, the more influential the parameter became (Cuntz et al., 2015). Because pet1 is directly related to evapotranspiration, which is the largest flux after precipitation in the water-balance equation, it was more influential in summer. Parameter sm10, a multiplier for saturated hydraulic conductivity, which influences the infiltration rate, became more influential during precipitation and snowmelt. The soil-moisture-related parameter sm17 was influential, but it was not for Yang et al. (2018), which indicates a larger influence of infiltration in the lowland part of the Bode catchment than in the Selke sub-catchment. Based on the sensitivity analysis, the top ten hydrological parameters and top five nitrate parameters were selected for model calibration.

Table 1. Description of parameters calibrated in the mHM-Nitrate model, their initial ranges and optimal values.

Process	Parameter	Description	Initial range	Optimal value
PET	pet1 (Shevenell, 1999)	Parameter for aspect correction of input potential evapotranspiration data	[6.99E-1, 1.30E+0]	9.80E-1
Soil moisture	sm10 (Cosby et al., 1984)	Transfer function parameter used to calculate soil saturated hydraulic conductivity	[-1.20E+0, -2.85E-1]	-8.42E-1
	sm17 (Brooks and Corey, 1964)	Parameter that determines the relative contribution of precipitation or snowmelt to runoff	[1.00E+0, 4.00E+0]	3.83E+0
	sm14 (Brooks and Corey, 1964)	Fraction of roots used to calculate actual evapotranspiration in forest areas	[9.00E-1, 9.99E-1]	9.73E-1
	sm16 (Brooks and Corey, 1964)	Fraction of roots used to calculate actual evapotranspiration in permeable areas	[1.00E-3, 8.99E-2]	5.63E-3
	sm4 (Cosby et al., 1984)	Pedotransfer function parameter used to calculate maximum soil moisture content	[6.46E-1, 9.51E-1]	9.44E-1
	sm11 (Cosby et al., 1984)	Pedotransfer function parameter used to calculate soil saturated hydraulic conductivity	[6.01E-3, 2.59E-2]	6.23E-3
Percolation	pc1	Parameter used to calculate the percolation coefficient	[0.00E+0, 5.00E+1]	1.44E+1
Interflow	intfl4	Slow interflow recession coefficient	[1.00E+0, 3.00E+1]	2.38E+1
	Intfl5	Slow interflow exponent coefficient	[5.00E-2, 2.99E-1]	5.55E-2

In-stream denitrification	deni_w	General parameter of in-stream denitrification rate (kg m^{-2} d^{-1})	[1.00E-8, 5.00E-2]	2.99E-4
Soil denitrification	deni_as	Soil denitrification rate on agricultural land (d^{-1})	[1.00E-8, 1.10E-1]	3.35E-3
	deni_s	Soil denitrification rate on non-agricultural land (d^{-1})	[1.00E-8, 1.10E-1]	5.50E-8
In-stream assimilation	pprt_aw	Primary production rate in agricultural streams (kg m^{-3} d^{-1})	[1.00E-8, 1.00E+0]	1.68E-1
	pprt_w	Primary production rate in non-agricultural streams (kg m^{-3} d^{-1})	[1.00E-8, 1.00E+0]	1.11E-1

3.2 Model performance

The mHM-Nitrate model reproduced the observed discharge and nitrate concentration at the six gauging stations reasonably well. Results for three typical gauging stations (Meisdorf, Hausneindorf and Stassfurt) are shown in this article, while those for other stations can be found in the Supplementary material. These three stations reflect different combinations of dominant land use and weather conditions from the upstream to downstream parts of the Bode catchment. Meisdorf represents a forest-dominated area, while Hausneindorf represents a mixture of forest and agricultural areas ranging from mountains to lowlands. In contrast, Stassfurt represents the whole catchment with a mixture of forest and agricultural areas.

Daily discharge predictions (Figure 3) and goodness-of-fit metrics (Table 2) showed that mHM-Nitrate captured discharge dynamics well during both calibration (2010-2014) and validation (2004-2009 and 2015-2018) periods (lowest NSE of 0.76 and 0.73, respectively). The model performed worse for the forest area than for the mixture of forest and agricultural areas. For example, the Meisdorf station had the lowest performance during the calibration period (KGE and PBIAS of 0.64 and -14.1%, respectively) and the first validation period (2004-2009) (KGE and PBIAS of 0.66 and -17%, respectively). The model performed best for all stations during the second validation period (2015-2018) (lowest NSE and KGE of 0.83 and 0.91, respectively; largest PBIAS of 1.6%) (Figure 3, Table 2).

The model represented seasonal dynamics in observed nitrate concentrations well (Figure 3). Nitrate concentrations had similar seasonal patterns as discharge during the study period, which reflects their control by hydrological processes. In the forest area (Meisdorf station), the model captured long-term nitrate concentration dynamics (2004-2018) reasonably well (lowest KGE of 0.66 and largest PBIAS of 23.70%) (Table 2). Model performance decreased for mixed forest and agricultural areas, as indicated by the lowest KGE values for nitrate concentrations at the Hausneindorf and Nienhagen stations (0.21 and 0.11, respectively).

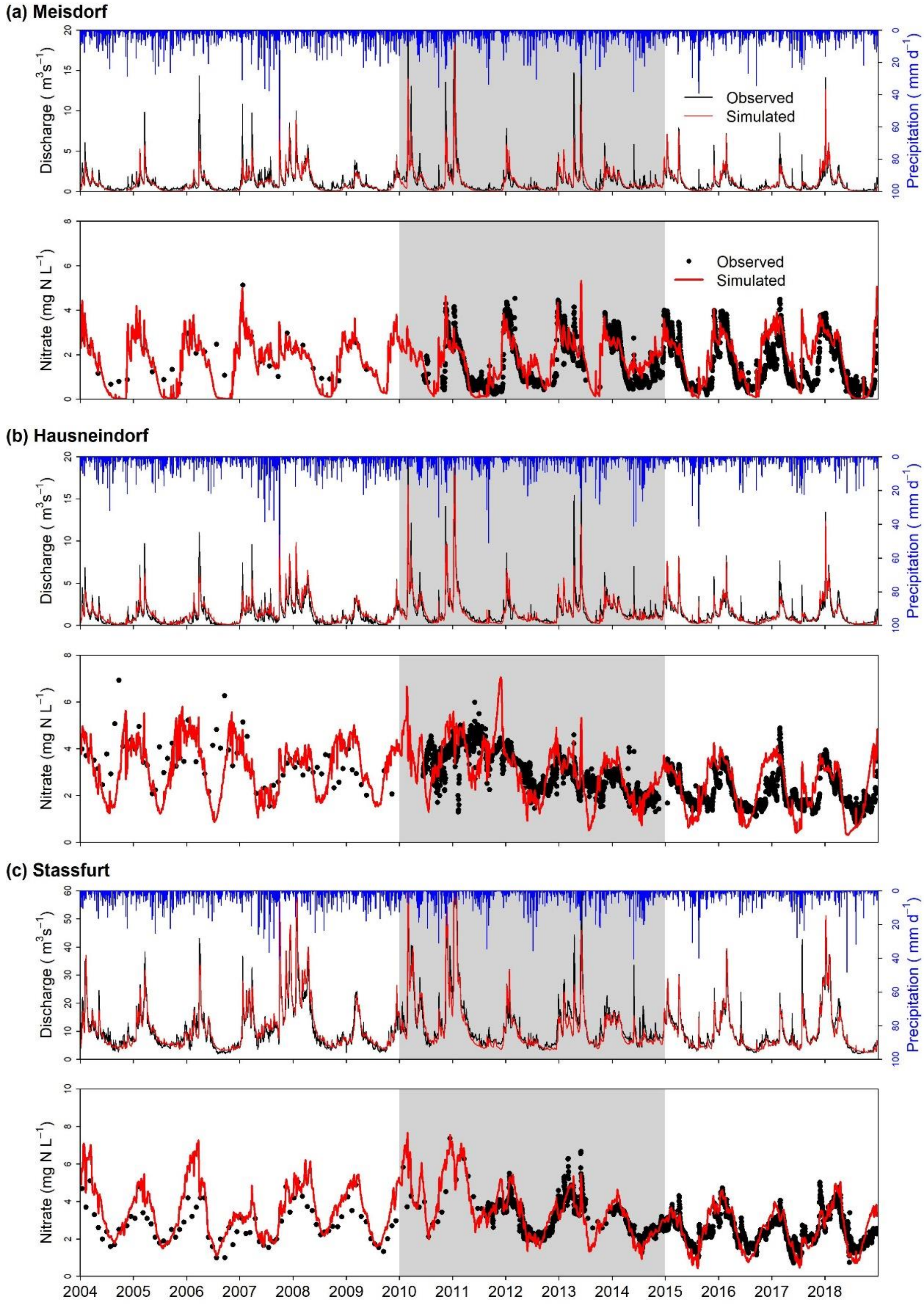

Figure 3. Observed and simulated daily discharge and nitrate concentration time series during the calibration (2010-2014) (shaded area) and validation period (2004-2009 and 2015-2018) at the three gauging stations: (a) Meisdorf, (b) Hausneindorf and (c) Stassfurt.

The model reproduced observed daily nitrate loads well for the Meisdorf, Hausneindorf and Stassfurt gauging stations, with the lowest coefficient of determination (R^2) of 0.73 (Figure S2). The model reproduced observed daily loads better for mixed forest and agricultural areas, represented by the Hausneindorf and Stassfurt stations (R^2 of 0.83 and 0.85, respectively). The lower performance for simulated daily loads in the forest area (i.e., Meisdorf station) can be explained by underestimating discharge during high flow periods (Figure 3a), which resulted in underestimating daily nitrate loads (Figure S2a). Like simulated discharge, the daily load was reproduced best during the second validation period (2015-2018) (NSE ranged from 0.81-0.92 and PBIAS ranged from -2 to 9.6 among the six gauging stations (Table 2).

Table 2. Model evaluation metrics (Nash-Sutcliffe Efficiency (NSE), Kling-Gupta Efficiency (KGE) and Percentage BIAS (PBIAS) for daily discharge (Q), nitrate concentration (Nitrate) and nitrate load (Load = Nitrate × Q) at the Meisdorf, Hausneindorf, Wegeleben, Nienhagen, Hadmersleben and Stassfurt gauging stations during the calibration (2010-2014) and validation periods (2004-2009 and 2015-2018).

Station	Criterion	Calibration			Validation					
		2010-2014			2004-2009			2015-2018		
		Q	Nitrate	Load	Q	Nitrate	Load	Q	Nitrate	Load
Meisdorf	NSE	0.77	0.59	0.66	0.73	0.35	0.88	0.83	0.40	0.81
	KGE	0.64	0.72	0.56	0.66	0.68	0.66	0.91	0.66	0.81
	PBIAS	-14.10	12.30	-12.60	-17.00	-10.20	-20.30	1.60	23.70	9.60
Hausneindorf	NSE	0.85	-0.35	0.80	0.74	-0.84	0.82	0.86	-0.70	0.84
	KGE	0.85	0.42	0.89	0.76	0.21	0.82	0.91	0.27	0.87
	PBIAS	-8.10	-0.10	-1.30	15.50	-8.70	15.70	-5.10	9.00	1.00
Wegeleben	NSE	0.91	-0.39	0.74	0.94	0.08	0.89	0.93	-	-
	KGE	0.90	0.48	0.74	0.92	0.40	0.91	0.91	-	-
	PBIAS	-7.90	-12.00	-16.00	-4.60	-4.90	-4.10	-3.40	-	-
Nienhagen	NSE	0.76	0.15	0.90	0.76	-0.34	0.81	-	-1.59	-
	KGE	0.85	0.72	0.83	0.78	0.50	0.82	-	0.11	-
	PBIAS	2.90	-19.60	-13.30	19.90	-10.50	13.20	-	-9.20	-
Hadmersleben	NSE	0.87	0.67	0.88	0.93	0.65	0.93	0.94	0.25	0.92
	KGE	0.90	0.74	0.92	0.94	0.76	0.81	0.95	0.61	0.93
	PBIAS	-7.40	3.00	-5.50	1.90	19.10	17.30	-4.30	11.10	4.60
Stassfurt	NSE	0.86	0.65	0.80	0.90	0.23	0.81	0.94	0.44	0.92
	KGE	0.89	0.77	0.73	0.91	0.61	0.67	0.95	0.59	0.96
	PBIAS	-8.50	1.70	-14.20	4.00	22.10	25.00	-3.50	1.60	-2.00

3.3 Discharge and nitrate concentration trends

To evaluate further the ability of mHM-Nitrate to simulate spatiotemporal nitrate dynamics in the Bode catchment, the trends of monthly mean observed and simulated nitrate concentrations at the three gauging stations were examined. The three components of monthly mean observed nitrate concentration showed the influence of trend, seasonal and random effects (Figure S3). The model captured the observed normalized monthly trends of nitrate concentration well (Figure 4) (Spearman's correlation coefficient of 0.54, 0.83 and 0.82 for Meisdorf, Hausneindorf and Stassfurt, respectively ($p < 0.01$)), indicating that the model successfully represented temporal dynamics of nitrate concentration trends at the three gauging stations. In addition, during 2004-2018, nitrate concentration decreased significantly ($p<0.05$) at Hausneindorf but non-significant at the Meisdorf and Stassfurt stations (Table S1).

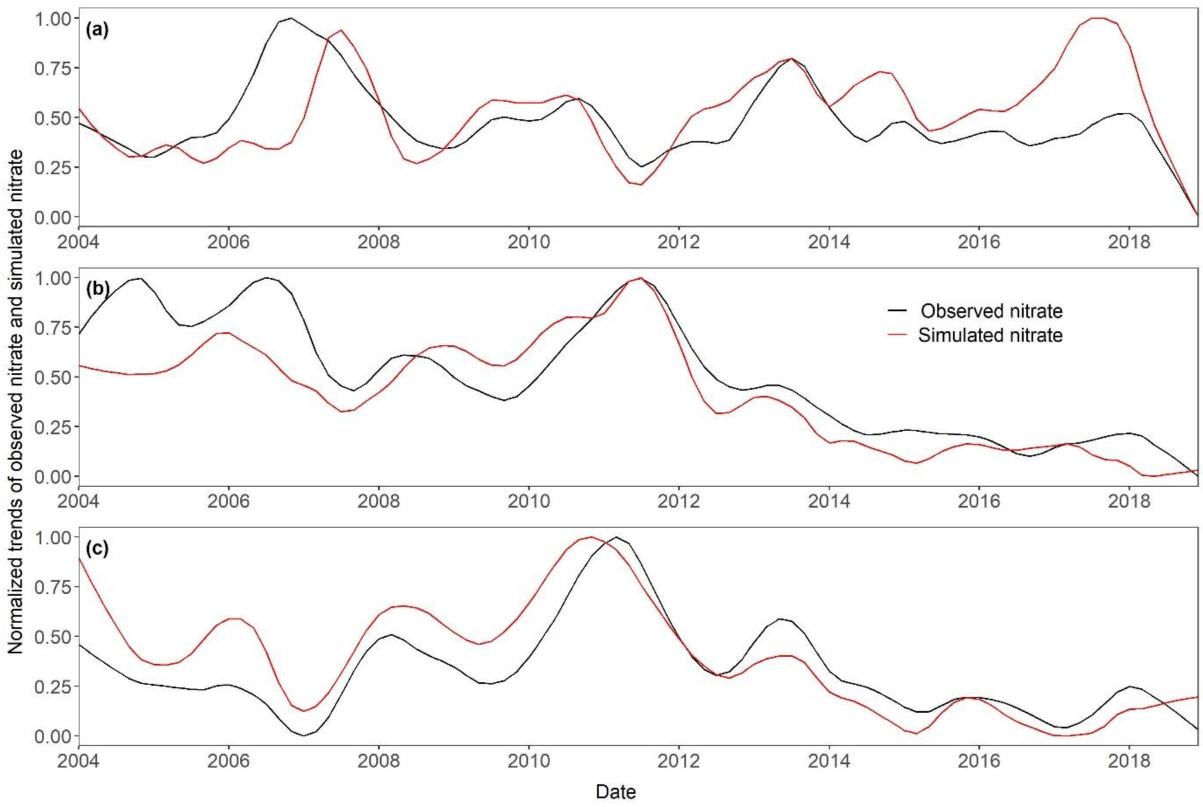

Figure 4. Normalized trends of monthly mean observed (aggregated from daily and monthly grab sampling data) nitrate concentration (black lines) and simulated (aggregated from daily

mHM-Nitrate model results) nitrate concentration (red lines) from 2004-2018 at the gauging stations (a) Meisdorf, (b) Hausneindorf and (c) Stassfurt.

The trends of monthly mean observed discharge and nitrate concentration were normalized at the Meisdorf, Hausneindorf and Stassfurt gauging stations from 2004-2018. Normalized trends of the monthly mean observed discharge and nitrate concentration were strongly correlated at Meisdorf and Stassfurt from 2004-2018 (Spearman's correlation coefficient of 0.65 and 0.59, respectively ($p < 0.01$)) (Figure 5), which indicates that hydrology influenced nitrate concentration strongly.

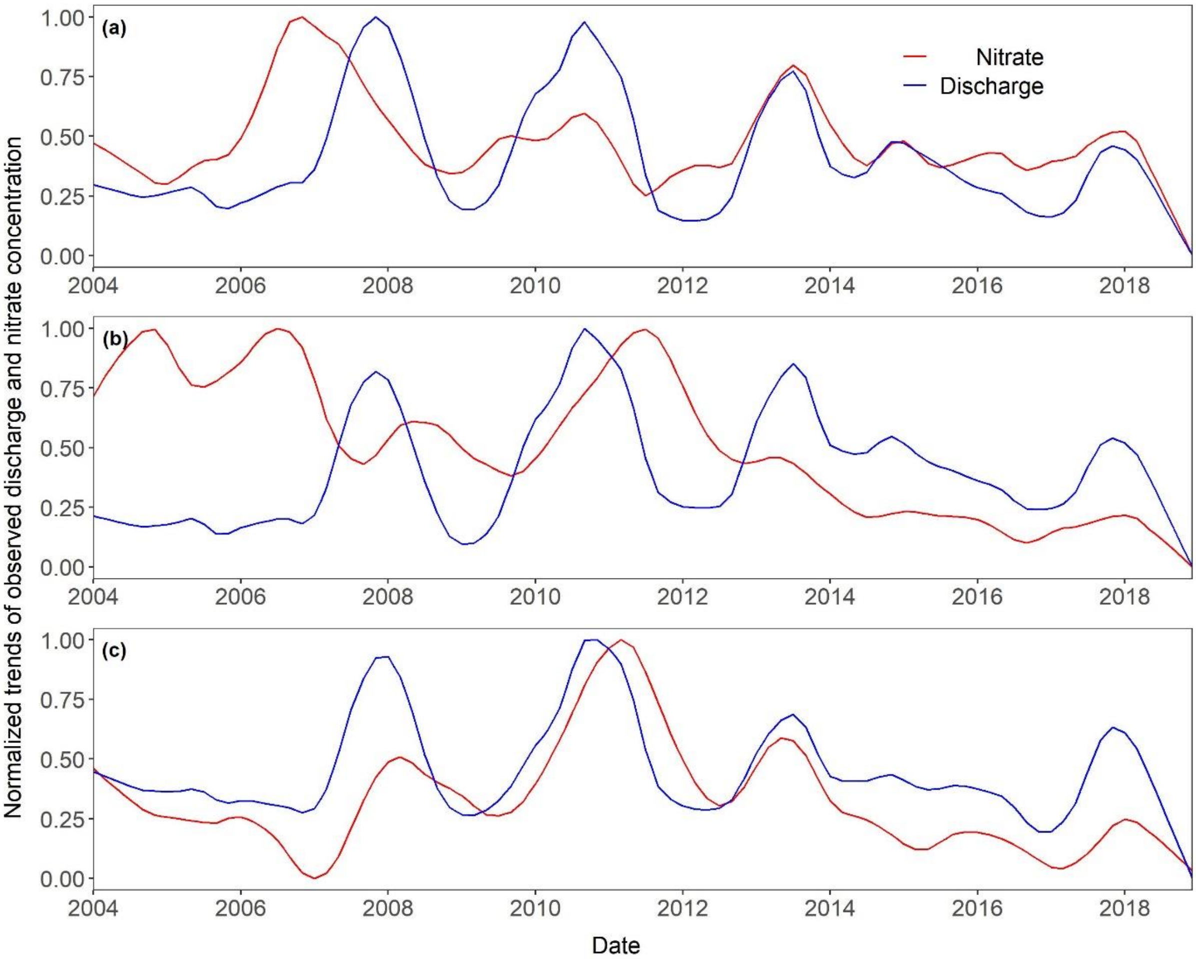

Figure 5. Normalized trends of monthly mean observed discharge (blue lines) and nitrate concentration (red lines) from 2004-2018 at the gauging stations (a) Meisdorf, (b) Hausneindorf and (c) Stassfurt.

3.4 Spatial heterogenous effects of drought on terrestrial nitrate export

The heterogeneous spatial changes in runoff components and thus nitrate concentrations (Figure S6) resulted in high spatial variability in nitrate load exported from the terrestrial compartment (Figure 6). The mean annual nitrate load in total runoff showed a spatial pattern that clearly depended on land use (Figure 6c), with the largest nitrate export from lowland agricultural area (Class I) and mountain pasture area (Class IV) (ca. 7 and 19 kg N ha^{-1} $year^{-1}$, respectively, Figure S7). The mean annual nitrate load in baseflow showed a similar spatial pattern (Figures 6b vs. 6c), with a mean of 5 and 6 kg N ha^{-1} $year^{-1}$ in Classes I and IV, respectively. In the 2015-2018 drought period, the nitrate load in total runoff decreased by a mean of 40% (Figure 6f), mainly due to the decreased nitrate export loads from interflow and baseflow in the lowland area (Figures 6d-e). For example, nitrate loads in interflow and baseflow decreased by 72% and 77%, respectively, in Class II, but they increased in baseflow by 16% in Class IV. The increased nitrate load of interflow, baseflow and total runoff in the mountain area during the drought period were due to higher nitrate concentration in interflow, baseflow and total runoff in these areas (Figures S6n-p).

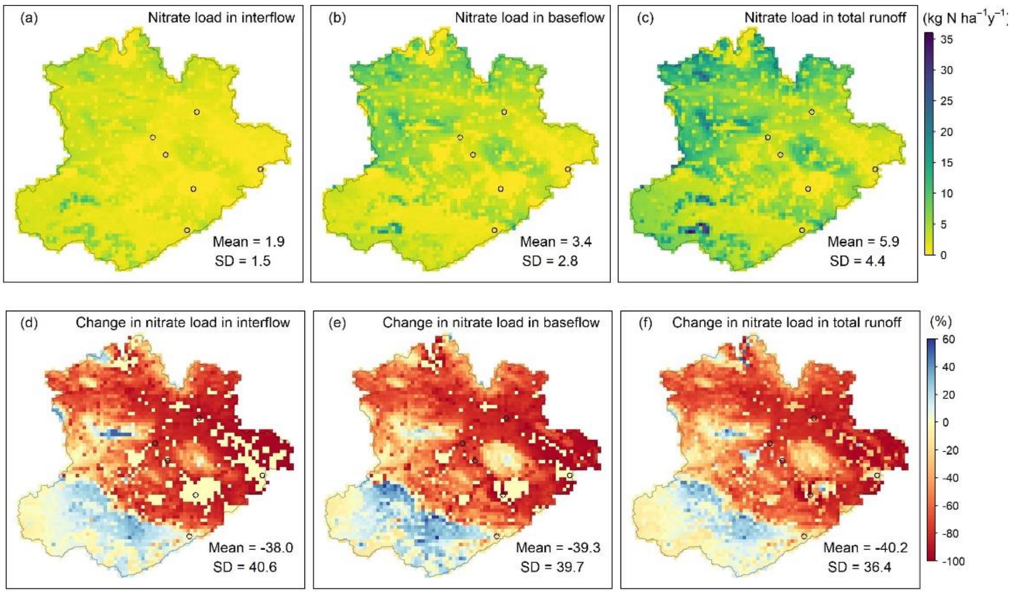

Figure 6. Spatial distribution of simulated (a-c) annual mean load of interflow, baseflow and total runoff from 2004-2014 and (d-f) the corresponding change from 2015-2018 compared to 2004-2014.

3.5 Drought effects on N surplus among soil-land-use classes

To identify the internal processes that influence nitrate dynamics in the Bode catchment better, soil N sources and sinks for the five soil-land-use classes were examined. For the agriculture-dominated lowland Classes I-III, the N source was mainly fertiliser (including mineral fertiliser and mineralized organic manure), which decreased slightly (by 5%) during the drought period compared to the pre-drought period (Table 3). It is noteworthy that the decreased fertiliser is due to different crop rotations during the drought period compared to pre-drought period. Crop uptake was the main N sink (83-90% of the total fertiliser amount) in Classes I-III, and it decreased slightly (ca. 10%) during the drought period compared to the pre-drought period. Soil denitrification, which can include denitrification in the upper groundwater when the water table is high, decreased considerably in Classes II and III (by 28% and 43%, respectively). This was likely due to lower soil moisture induced by drought in the lowland, which decreased crop uptake and soil denitrification during the drought period. Terrestrial export also decreased greatly in Classes I-III. Therefore, soil N surplus, which equals input (total fertiliser amount and precipitation deposition) minus output (crop/plant uptake) was higher in Classes I-II (by 4.4 and 3.1 kg N ha^{-1} y^{-1}, respectively) during the drought period than the pre-drought period, indicating that more N was stored in the soil in the lowland area during the drought period.

In the mountain area, N sources and sinks in Classes IV and V responded differently to drought than these of Classes I-III (Table 3). The total amount of fertiliser in Classes IV and V remained relatively constant during the drought period. Class IV had the lowest soil denitrification among the five classes, perhaps due to lower total fertiliser amount and lower temperature in mountain pastures. In addition, soil denitrification and terrestrial export in Classes IV and V did not change during the 2015-2018 drought period compared to the 2004-2014 period, which indicates that drought had less effect in the mountain area.

Table 3. N balances (mean ± standard deviation) in the five soil-land-use classes during the 2004-2014 pre-drought period and, in parentheses, their corresponding values in the 2015-2018 drought period.

N balances	Soil-land-use classes					
(kg N ha^{-1} y^{-1})	I	II	III	IV	V*	Catchment mean
Total fertiliser amount	172.5 ± 8.2 (163.1 ± 7.7)	168.8 ± 10.0 (159.6 ± 9.4)	170.5 ± 9.2 (161.3 ± 8.7)	63.8 ± 16.4 (64.2 ± 16.9)	158.3 (163.5)	113.0 ± 69.8 (107.4 ± 65.6)
Precipitation deposition	11.7 ± 0.6 (9.9 ± 1.1)	11.2 ± 0.5 (9.2 ± 0.9)	11.0 ± 0.2 (8.7 ± 0.3)	17.7 ± 0.4 (16.7 ± 0.4)	14.7 (13.7)	13.2 ± 3.3 (11.5 ± 3.4)
Crop/plant uptake	142.8 ± 6.8 (127.2 ± 6.9)	142.6 ± 8.0 (128.3 ± 8.0)	154.1 ± 6.6 (143.6 ± 7.6)	39.8 ± 17.6 (37.3 ± 15.8)	121.2 (106.4)	96.4 ± 55.2 (86.7 ± 49.0)
Soil denitrification	34.2 ± 3.3 (28.1 ± 5.6)	32.5 ± 4.5 (23.4 ± 5.3)	21.0 ± 4.4 (12.8 ± 2.0)	2.5 ± 3.5 (2.6 ± 3.7)	24.0 (25.0)	20.3 ± 15.2 (16.7 ± 13.0)
Terrestrial export	7.2 ± 3.6 (3.2 ± 3.2)	4.0 ± 2.6 (1.2 ± 1.8)	0.3 ± 0.2 (0.02 ± 0.02)	19.4 ± 3.5 (20.3 ± 2.3)	12.1 (13.5)	6.0 ± 4.1 (3.7 ± 3.7)

*Note that for Class V only one grid was selected.

3.6 Drought effects on in-stream nitrate retention

Annual and seasonal mean lateral nitrate loading from terrestrial to streams decreased during the drought period compared to the pre-drought period, except for the streams upstream of Meisdorf (Table 4). Lateral nitrate loading reduced by 41% and 44% in summer and autumn within the whole river network; meanwhile, in-stream retention amount decreased by 20% and 16%, respectively, plausibly due to smaller stream benthic area and lower nitrate concentrations during the drought period. Lateral nitrate loading reduced more than that of in-stream retention during the drought period, and this resulted in a higher in-stream retention efficiency (Table 4).

Table 4. Seasonal and annual mean values of nitrate loading and in-stream retention at station Meisdorf (Meis), Hausneindorf (Haus) and Stassfurt (Stass) during the 2004-2014 pre-drought period and, in parentheses, their corresponding values in the 2015-2018 drought period.

	Winter			Spring			Summer			Autumn			Annual		
Load/In-stream retention (kg N d^{-1})	Meis	Haus	Stass	Meis	Haus	Stass	Meis	Haus	Stass	Meis	Haus	Stass	Meis	Haus	Stass
Load	423.3	837.8	7848.9	317.8	730.0	6947.1	103.0	299.9	2972.9	126.3	332.0	3324.3	229.5	539.0	5249.5
	(554.7)	(746.1)	(5529.2)	(303.2)	(468.8)	(4044.1)	(56.2)	(157.6)	(1758.5)	(91.7)	(178.5)	(1853.8)	(238.3)	(375.2)	(3233.8)
Retention	5.7	19.1	211.5	35.3	117.1	1232	33.7	143.0	1671.4	16.2	61.3	728.4	22.4	83.9	947.7
	(8.9)	(25.8)	(267.2)	(39.2)	(113.6)	(1124.5)	(28.1)	(98.5)	(1332.4)	(16.0)	(50.4)	(615.2)	(22.7)	(71.1)	(823.4)
Percentage of retention	1.4	2.3	2.7	11.1	16.0	17.7	32.7	47.7	56.2	12.8	18.5	21.9	9.8	15.6	18.1
(%)	(1.6)	(3.5)	(4.8)	(12.9)	(24.2)	(27.8)	(50.0)	(62.5)	(75.8)	(17.5)	(28.2)	(33.2)	(9.5)	(18.9)	(25.5)

Note. The load was the sum of model-simulated total terrestrial loads from the drainage area upstream of each station, and in-stream retention was the sum of net assimilation uptake and denitrification amount from the stream network upstream of each station.

4. Discussion

4.1 Model performance evaluation

The mHM-Nitrate model reproduced the observed discharge throughout the Bode catchment well (mean NSE of 0.85 and PBIAS ≤ ±20%), according to guidelines for evaluating the performance of catchment simulations (Moriasi et al., 2015). This accuracy is similar to those of previous simulations of the study area (e.g., Mueller et al., 2016; Nguyen et al., 2021; Yang et al., 2018). Comparing the three representative gauging stations, the performance at the Meisdorf station was relatively low, as indicated by lower NSE and KGE (Table 1), perhaps due to underestimating peak flow events and the high sensitivity of NSE to extreme values (e.g., Krause et al., 2005). Similarly, the low KGE was likely due to underestimating high flow values in 2010, 2013 and 2014 (Figure 3a).

The model may have underestimated peak flow events because of the inaccurately measured precipitation and the lower density of meteorological stations. Specifically, daily precipitation is not sufficiently precise to represent a detailed discharge response, especially in the headwater of the Bode catchment (due to high heterogeneity in precipitation), where many storm events last only a few hours. Moreover, the spatial coverage of the meteorological stations decreased significantly during the recent period, especially in the mountain area of the catchment. For example, the number of precipitation gauging stations in the Selke sub-catchment decreased from 16 to only 8 after 2004 (Yang et al., 2018). Generally, the decrease in detailed precipitation records decreased performance in predicting discharge in the headwater area, which is known for its high spatiotemporal variability in precipitation due to the varying elevation. Therefore, the less accurate precipitation inputs from the lower station density could explain the slight underestimate of water balance at Meisdorf (PBIAS of -14% and -17% for the calibration and first validation period, respectively).

However, the model slightly overestimated the water balance for the Hausneindorf station during the first validation period (Table 2). Jiang et al. (2014) and Winter et al. (2021) stated that water from the lower Selke River was abstracted to fill pit lakes from 1998-2009 at a rate of 3.1 million m^3 $year^{-1}$, which was ca. 8% of the mean annual stream flow from 2004-2009. Although the water balance remained overestimated after considering this abstraction, these overestimates occurred mainly during the low-flow period and were acceptable when the corresponding runoff depth was considered (i.e., the largest PBIAS of 15.5% at Hausneindorf corresponded to a runoff depth of only 12.8 mm/year).

Although NSE values were negative at Hausneindorf and Nienhagen stations during validation periods (Table 2), due to few extreme values (Krause et al., 2005; Moriasi et al., 2015). With regard to the KGE and PBIAS values at these two stations, the model performance was acceptable. The slightly lower performance of mHM-Nitrate at the Hausneindorf and Nienhagen stations than at the other stations was likely due to the lack of detailed time series of point sources from urban areas during the low-flow period, especially in the initial period of operation of the WWTPs, as they started to function properly only in 2007 (Yang et al., 2018). The high nitrate concentrations during summers before 2007 (Figure 3b) were likely caused by untreated point sources, as discussed in Yang et al. (2018). After 2007, the model captured the dynamics of nitrate concentration well at Hausneindorf station. In addition, some houses (mainly summer houses) in the Selke sub-catchment are not connected to the sewage system, which may generate additional unknown point sources and can decrease model performance under low-flow conditions. The lack of detailed spatial cropping information for the entire Bode catchment and the need to rely on only rough survey information might introduce additional uncertainty. Nevertheless, mHM-Nitrate successfully identified decreasing trends in observed nitrate concentrations at the Hausneindorf and Stassfurt lowland stations (Figures 3 and 4). The model performance was in line with that of

Yang et al. (2018) in the Selke sub-catchment, and they also confirmed that the simulations based on DDS calibration performed similarly good with that of using the DREAM method.

The model can represent observed nitrate concentrations well for several reasons. First, its flexible structure ensures sufficient spatial representation of catchment heterogeneity as well as spatiotemporal variability in meteorological inputs (Kumar et al., 2010; Samaniego et al., 2010; Yang et al., 2018). In addition, it can adequately represent the diffuse source inputs and turnover (i.e., agricultural practices, crop rotation and plant uptake) and point-source contributions (input time series can be added at the real stream locations) at the resolution of the input data, which increases the model's ability to represent spatial variability in nitrate sources (Yang et al., 2018). Selecting an appropriate calibration period under varying conditions (e.g., at nonstationary conditions like the drought) is crucial for model training. For example, during the calibration period, 2011 was a wetter year, while 2012 was a drier year. Thus, selecting a calibration period that encompasses varying hydrological conditions helps activate all model components. This approach agrees with Engel et al. (2007), who suggested that both calibration and validation periods should have high and low flows to increase a model's robustness. Together, these characteristics helped to identify model parameters better and reliably estimate nitrate contributions from different runoff components, which is crucial for representing nitrate concentrations spatiotemporally in the entire Bode catchment.

The most influential nitrate sub-model parameter was related to in-stream denitrification, while in the study of Yang et al. (2018), which focused more on upstream catchments, the most influential parameter was related to soil denitrification. This is presumably due to the larger total stream benthic areas for the Bode catchment, which is in line with Yang et al. (2019b) who found that there is a significant relationship between stream benthic area and in-stream denitrification rate, reflecting the relative increasing importance of in-stream processes with increasing catchment size.

4.2 Explaining changes in nitrate concentration during drought years

Recent droughts (2015-2018) in the Bode catchment provided an opportunity to investigate the internal processes that influence nitrate dynamics under changing weather conditions at the catchment scale. Observed nitrate concentration showed a decreasing trend in lowland agricultural areas (i.e., Hausneindorf and Stassfurt stations) but not significant in the mountain forest area (i.e., Meisdorf station) (Figure 4). Results suggested that the influence of drought on nitrate concentration could be explained by (i) spatiotemporal differences in hydrological response and (ii) its associated effects on soil and in-stream nitrate processes during the 2015-2018 drought period compared to the 2004-2014 pre-drought period.

Seasonal total runoff decreased in the entire Bode catchment during the drought period (Figures S8m-p). The decrease was larger in the lowland area, due to the combined effects of meteorology and soil properties. Annual precipitation in the 2015-2018 drought period did not differ greatly from that in long-term historical records (1971-2000) from DWD. When considering the temporal distribution of precipitation, however, precipitation decreased greatly in winter and spring in the lowland agricultural area during the drought period, especially in Class II (by 25% and 30%, respectively) (Figures S8a-b). Soil moisture decreased continuously in all seasons and was not replenished during the rewetting seasons due to reduced precipitation in the lowland area (Figures S8i-l). In addition, the modeled soil moisture of the third layer in Classes (I-III) showed a significant decline during drought period (Figure S9).

Consequently, this process could decrease unsaturated zone storage and groundwater recharge during the drought period. This further explains the decrease in mean annual interflow, baseflow and total runoff in the lowland area during the 2015-2018 drought period compared to 2004-2014. Furthermore, the decrease in soil moisture content may have decreased hydrological connectivity between hillslope and streams during the drought period (Figures S6f-h), thus increasing the potential for soil profiles to become disconnected from the stream channel and shallow groundwater (Davis et al., 2014; Outram et al., 2016). In contrast, total runoff in the mountain area decreased only slightly during the drought period, perhaps due to seasonal precipitation and slightly decreased soil moisture content there (Figure S8). This result agrees with other studies that reported that flatter and less forested catchments are more vulnerable to long-term drought (Saft et al., 2015).

The large decrease in nitrate concentration in the lowland area during the drought period, represented by the Hausneindorf and Stassfurt stations (Figures 4b-c), was plausible because the decrease in interflow, baseflow and total runoff in Classes I-III greatly reduced soil nitrate export from interflow and baseflow which are the major source of the terrestrial nitrate export to surface water (Figures 6d-f, Table 3). This indicates that nitrate became more transport-limited in the lowland area during the drought period. In addition, upstream discharge with low nitrate concentration could dilute downstream nitrate concentration. The share of discharge from uplands (sum of discharge at Thale and Meisdorf station) to the total discharge at the outlet of the Bode catchment increased from 44.3% to 48.8% from the pre-drought period to the drought period. Furthermore, drought increased water temperatures, and longer stream water residence time in summer could have stimulated in-stream uptake and denitrification efficiency (Table 4) (Hosen et al., 2019; Rode et al., 2016). Therefore, the combined effects of terrestrial export load and in-stream processes could explain the decrease of in-stream nitrate concentrations in lowland areas (e.g., at the Hausneindorf and Stassfurt stations in Figures 4b-c). In contrast, nitrate concentration in the mountain forest-dominated area showed a constant pattern during the drought period compared to the pre-drought period, as reflected by the Meisdorf station (Figures 3a and 4a). This pattern could have occurred because the share of discharge from high nitrate concentration agricultural areas and low nitrate concentration forest areas did not change substantially (Figure 6 and Table 3). Nitrate source in the mountain forest-dominated area comes mainly from patches of agricultural area, which decreased slightly during the drought period in Class IV (Table 3). Although total runoff increased in the mountain area in winter during the drought period, in-stream nitrate concentrations were similar to those during the pre-drought period (Figures S8m vs. 3a). In addition, in-stream retention in winter was low and did not influence nitrate concentration, which indicated that nitrate could be supply-limited in the mountain area.

Previous studies have reported a decrease in stream nitrate concentrations during droughts (e.g., van Vliet and Zwolsman, 2008; Yevenes et al., 2018). They also explained the decrease in nitrate concentration by less diffuse supply based on empirical relations between nitrate concentration and discharge. Our study confirmed this explanation by simulating a large decrease in soil nitrate export in the lowland area during the drought period (Figure 6).

5. Conclusion

Varying spatial trends in nitrate concentration under drought conditions were observed in the Bode catchment in central Germany. To explain the mechanisms that influence the changes in trends, calibrated mHM-Nitrate model outputs and internal processes were compared between a drought period (2015-2018) and a pre-drought period (2004-2014). Results indicated that nitrate export from the terrestrial compartment greatly decreased while in-stream retention efficiency increased during the drought periods, which could result in the decrease of in-stream nitrate concentration in the lowland area of the Bode catchment. In contrast, nitrate export and in-stream retention efficiency in the upper mountain area of the catchment changed little. Therefore, nitrate concentrations remained relatively constant in the drought and pre-drought periods. Results suggested that during the drought periods, nitrate was mainly stored in the soil rather than mobilized or transported, especially in the lowland area of the catchment. This study assessed the model's ability to represent nitrate concentrations under varying weather conditions, which could be used to study the effects of climate change. The Bode catchment is a typical mesoscale catchment in central Europe, in which the headwater is a mountain area with high precipitation, and the lowland is an agricultural area with relatively low precipitation. We expect that catchments with landscape and climate conditions similar to those of the Bode catchment (i.e., wet mountain areas and dry lowland areas) are highly vulnerable to changing weather conditions. This study showed that droughts have heterogeneous spatial effects on hydrology and water-quality responses. Therefore, water managers should specifically consider this spatial heterogeneity when managing future droughts.

Acknowledgements

X. Zhou is funded by the Chinese Scholarship Council (CSC). We thank the German Weather Service (DWD), Federal Institute for Geosciences and Natural Resources (BGR) and State Agency for Flood Protection and Water Management of Saxony-Anhalt (LHW) for providing meteorological, geological and discharge and water-quality data, respectively. The high-frequency nitrate-concentration data were provided by the TERENO (Terrestrial Environment Observatories) project.

Data Availability Statement

The model code of mHM-Nitrate is publicly available at https://zenodo.org/record/3891629.

References

Baldwin, D.S., Rees, G.N., Mitchell, A.M. and Watson, G. 2005. Spatial and temporal variability of nitrogen dynamics in an upland stream before and after a drought. Marine and Freshwater Research 56(4), 457-464.

Ballard, T.C., Sinha, E. and Michalak, A.M. 2019. Long-Term Changes in Precipitation and Temperature Have Already Impacted Nitrogen Loading. Environ Sci Technol 53(9), 5080-5090.

Brooks, R.H. and Corey, A.T. 1964. Hydraulic properties of porous media. Hydrology papers (Colorado State University); no. 3.

Cleveland, R.B., Cleveland, W. S., McRae, J. E., & Terpenning, I. J. 1990. STL: A seasonal-trend decomposition procedure based on loess. Journal of Official Statistics 6.

Cosby, B.J., Hornberger, G.M., Clapp, R.B. and Ginn, T.R. 1984. A Statistical Exploration of the Relationships of Soil-Moisture Characteristics to the Physical-Properties of Soils. Water Resources Research 20(6), 682-690.

Cuntz, M., Mai, J., Zink, M., Thober, S., Kumar, R., Schäfer, D., Schrön, M., Craven, J., Rakovec, O., Spieler, D., Prykhodko, V., Dalmasso, G., Musuuza, J., Langenberg, B., Attinger, S. and Samaniego, L. 2015. Computationally inexpensive identification of noninformative model parameters by sequential screening. Water Resources Research 51(8), 6417-6441.

Davis, C.A., Ward, A.S., Burgin, A.J., Loecke, T.D., Riveros-Iregui, D.A., Schnoebelen, D.J., Just, C.L., Thomas, S.A., Weber, L.J. and St. Clair, M.A. 2014. Antecedent Moisture Controls on Stream Nitrate Flux in an Agricultural Watershed. Journal of Environmental Quality 43(4), 1494-1503.

Engel, B., Storm, D., White, M., Arnold, J. and Arabi, M. 2007. A hydrologic/water quality model application protocol. Journal of the American Water Resources Association 43(5), 1223-1236.

George, H.H. and Zohrab, A.S. 1985. Reference Crop Evapotranspiration from Temperature. Applied Engineering in Agriculture 1(2), 96-99.

Gupta, H.V., Kling, H., Yilmaz, K.K. and Martinez, G.F. 2009. Decomposition of the mean squared error and NSE performance criteria: Implications for improving hydrological modelling. Journal of Hydrology 377(1-2), 80-91.

Hanel, M., Rakovec, O., Markonis, Y., Maca, P., Samaniego, L., Kysely, J. and Kumar, R. 2018. Revisiting the recent European droughts from a long-term perspective. Sci Rep 8(1), 9499.

Hari, V., Rakovec, O., Markonis, Y., Hanel, M. and Kumar, R. 2020. Increased future occurrences of the exceptional 2018-2019 Central European drought under global warming. Sci Rep 10(1), 12207.

Hesse, C. and Krysanova, V. 2016. Modeling Climate and Management Change Impacts on Water Quality and In-Stream Processes in the Elbe River Basin. Water 8(2).

Hosen, J.D., Aho, K.S., Appling, A.P., Creech, E.C., Fair, J.H., Hall, R.O., Kyzivat, E.D., Lowenthal, R.S., Matt, S., Morrison, J., Saiers, J.E., Shanley, J.B., Weber, L.C., Yoon, B. and Raymond, P.A. 2019. Enhancement of primary production during drought in a temperate watershed is greater in larger rivers than headwater streams. Limnology and Oceanography 64(4), 1458-1472.

Huang, S., Krysanova, V. and Hattermann, F. 2015. Projections of climate change impacts on floods and droughts in Germany using an ensemble of climate change scenarios. Regional Environmental Change 15(3), 461-473.

Hundecha, Y. and Bárdossy, A. 2004. Modeling of the effect of land use changes on the runoff generation of a river basin through parameter regionalization of a watershed model. Journal of Hydrology 292(1-4), 281-295.

Jarvis, A., H.I. Reuter, A. Nelson, E. Guevara. 2008 Hole-filled SRTM for the globe Version 4, available from the CGIAR-CSI SRTM 90m Database http://srtm.csi.cgiar.org/.

Jiang, S.Y., Jomaa, S. and Rode, M. 2014. Modelling inorganic nitrogen leaching in nested mesoscale catchments in central Germany. Ecohydrology 7(5), 1345-1362.

Krause, P., Boyle, D.P. and Bäse, F. 2005. Comparison of different efficiency criteria for hydrological model assessment. Advances in Geosciences 5, 89-97.

Kumar, R., Samaniego, L. and Attinger, S. 2010. The effects of spatial discretization and model parameterization on the prediction of extreme runoff characteristics. Journal of Hydrology 392(1-2), 54-69.

Leitner, S., Dirnbock, T., Kobler, J. and Zechmeister-Boltenstern, S. 2020. Legacy effects of drought on nitrate leaching in a temperate mixed forest on karst. J Environ Manage 262, 110338.

Lindström, G., Pers, C., Rosberg, J., Strömqvist, J. and Arheimer, B. 2010. Development and testing of the HYPE (Hydrological Predictions for the Environment) water quality model for different spatial scales. Hydrology Research 41(3-4), 295-319.

Lintern, A., Webb, J.A., Ryu, D., Liu, S., Waters, D., Leahy, P., Bende-Michl, U. and Western, A.W. 2018. What Are the Key Catchment Characteristics Affecting Spatial Differences in Riverine Water Quality? Water Resources Research 54(10), 7252-7272.

Lutz, S.R., Mallucci, S., Diamantini, E., Majone, B., Bellin, A. and Merz, R. 2016. Hydroclimatic and water quality trends across three Mediterranean river basins. Sci Total Environ 571, 1392-1406.

Moriasi, D.N., Gitau, M.W., Pai, N. and Daggupati, P. 2015. Hydrologic and Water Quality Models: Performance Measures and Evaluation Criteria. Transactions of the Asabe 58(6), 1763-1785.

Morris, M.D. 1991. Factorial sampling plans for preliminary computational experiments. Technometrics 33(2), 161-174.

Mosley, L.M. 2015. Drought impacts on the water quality of freshwater systems; review and integration. Earth-Science Reviews 140, 203-214.

Mueller, C., Zink, M., Samaniego, L., Krieg, R., Merz, R., Rode, M. and Knoller, K. 2016. Discharge Driven Nitrogen Dynamics in a Mesoscale River Basin As Constrained by Stable Isotope Patterns. Environ Sci Technol 50(17), 9187-9196.

Nguyen, T.V., Kumar, R., Lutz, S.R., Musolff, A., Yang, J. and Fleckenstein, J.H. 2021. Modeling Nitrate Export From a Mesoscale Catchment Using StorAge Selection Functions. Water Resources Research 57(2).

Outram, F.N., Cooper, R.J., Sünnenberg, G., Hiscock, K.M. and Lovett, A.A. 2016. Antecedent conditions, hydrological connectivity and anthropogenic inputs: Factors affecting nitrate and phosphorus transfers to agricultural headwater streams. Science of The Total Environment 545-546, 184-199.

Pianosi, F., Sarrazin, F. and Wagener, T. 2015. A Matlab toolbox for Global Sensitivity Analysis. Environ Modell Softw 70, 80-85.

R Core Team. 2020 R: A Language and Environment for Statistical Computing. Vienna, Austria: R Foundation for Statistical Computing. Available online: http://www.R-project.org/ (accessed on 09 September 2020).

Rahimi, S., Modin, O. and Mijakovic, I. 2020. Technologies for biological removal and recovery of nitrogen from wastewater. Biotechnol Adv 43, 107570.

Rode, M., Arhonditsis, G., Balin, D., Kebede, T., Krysanova, V., van Griensven, A. and van der Zee, S.E.A.T.M. 2010. New challenges in integrated water quality modelling. Hydrological Processes 24(24), 3447-3461.

Rode, M., Halbedel Nee Angelstein, S., Anis, M.R., Borchardt, D. and Weitere, M. 2016. Continuous In-Stream Assimilatory Nitrate Uptake from High-Frequency Sensor Measurements. Environ Sci Technol 50(11), 5685-5694.

Saft, M., Western, A.W., Zhang, L., Peel, M.C. and Potter, N.J. 2015. The influence of multiyear drought on the annual rainfall-runoff relationship: An Australian perspective. Water Resources Research 51(4), 2444-2463.

Samaniego, L., Kumar, R. and Attinger, S. 2010. Multiscale parameter regionalization of a grid-based hydrologic model at the mesoscale. Water Resources Research 46(5).

Shevenell, L. 1999. Regional potential evapotranspiration in arid climates based on temperature, topography and calculated solar radiation. Hydrological Processes 13(4), 577-596.

Spinoni, J., Vogt, J.V., Naumann, G., Barbosa, P. and Dosio, A. 2018. Will drought events become more frequent and severe in Europe? International Journal of Climatology 38(4), 1718-1736.

Stow, C.A., Cha, Y., Johnson, L.T., Confesor, R. and Richards, R.P. 2015. Long-Term and Seasonal Trend Decomposition of Maumee River Nutrient Inputs to Western Lake Erie. Environmental Science & Technology 49(6), 3392-3400.

Stow, C.A., Dyble, J., Kashian, D.R., Johengen, T.H., Winslow, K.P., Peacor, S.D., Francoeur, S.N., Burtner, A.M., Palladino, D., Morehead, N., Gossiaux, D., Cha, Y., Qian, S.S. and Miller, D. 2014. Phosphorus targets and eutrophication objectives in Saginaw Bay: A 35year assessment. Journal of Great Lakes Research 40, 4-10.

Tolson, B.A. and Shoemaker, C.A. 2007. Dynamically dimensioned search algorithm for computationally efficient watershed model calibration. Water Resources Research 43(1).

UBA (2019) 2019 Monitoring Report on the German Strategy for Adaptation to Climate Change,https://www.umweltbundesamt.de/en/publikationen/2019-monitoring-report.

van Vliet, M.T.H. and Zwolsman, J.J.G. 2008. Impact of summer droughts on the water quality of the Meuse river. Journal of Hydrology 353(1-2), 1-17.

Vicente-Serrano, S.M., Begueria, S. and Lopez-Moreno, J.I. 2010. A Multiscalar Drought Index Sensitive to Global Warming: The Standardized Precipitation Evapotranspiration Index. Journal of Climate 23(7), 1696-1718.

Wellen, C., Kamran-Disfani, A.R. and Arhonditsis, G.B. 2015. Evaluation of the current state of distributed watershed nutrient water quality modeling. Environ Sci Technol 49(6), 3278-3290.

Whitehead, P.G., Wilby, R.L., Battarbee, R.W., Kernan, M. and Wade, A.J. 2009. A review of the potential impacts of climate change on surface water quality. Hydrological Sciences Journal 54(1), 101-123.

Winter, C., Lutz, S.R., Musolff, A., Kumar, R., Weber, M. and Fleckenstein, J.H. 2021. Disentangling the Impact of Catchment Heterogeneity on Nitrate Export Dynamics From Event to Long-Term Time Scales. Water Resources Research 57(1).

Wollschläger, U., Attinger, S., Borchardt, D., Brauns, M., Cuntz, M., Dietrich, P., Fleckenstein, J.H., Friese, K., Friesen, J., Harpke, A., Hildebrandt, A., Jäckel, G., Kamjunke, N., Knöller, K., Kögler, S., Kolditz, O., Krieg, R., Kumar, R., Lausch, A., Liess, M., Marx, A., Merz, R., Mueller, C., Musolff, A., Norf, H., Oswald, S.E., Rebmann, C., Reinstorf, F., Rode, M., Rink, K., Rinke, K., Samaniego, L., Vieweg, M., Vogel, H.-J., Weitere, M., Werban, U., Zink, M. and Zacharias, S. 2016. The Bode hydrological observatory: a platform for integrated, interdisciplinary hydro-ecological research within the TERENO Harz/Central German Lowland Observatory. Environmental Earth Sciences 76(1).

Yang, X., Jomaa, S., Buttner, O. and Rode, M. 2019a. Autotrophic nitrate uptake in river networks: A modeling approach using continuous high-frequency data. Water Res 157, 258-268.

Yang, X., Jomaa, S. and Rode, M. 2019b. Sensitivity Analysis of Fully Distributed Parameterization Reveals Insights Into Heterogeneous Catchment Responses for Water Quality Modeling. Water Resources Research 55(12), 10935-10953.

Yang, X., Jomaa, S., Zink, M., Fleckenstein, J.H., Borchardt, D. and Rode, M. 2018. A New Fully Distributed Model of Nitrate Transport and Removal at Catchment Scale. Water Resources Research.

Yang, X. and Rode, M. 2020 A Fully Distributed Catchment Nitrate Model - mHM-Nitrate v2.0.

Yevenes, M.A., Figueroa, R. and Parra, O. 2018. Seasonal drought effects on the water quality of the Biobio River, Central Chile. Environ Sci Pollut Res Int 25(14), 13844-13856.

Zwolsman, J.J.G. and van Bokhoven, A.J. 2007. Impact of summer droughts on water quality of the Rhine River - a preview of climate change? Water Science and Technology 56(4), 45-55.